Supplement of Atmos. Meas. Tech., 11, 1689–1705, 2018
https://doi.org/10.5194/amt-11-1689-2018-supplement


Atmospheric Measurement Techniques
Open Access

*Supplement of*

# Atmospheric characterization through fused mobile airborne and surface in situ surveys: methane emissions quantification from a producing oil field

**Ira Leifer et al.**

*Correspondence to:* Ira Leifer (ira.leifer@bubbleology.com)

**Supplemental Material**

## S1. Study Area

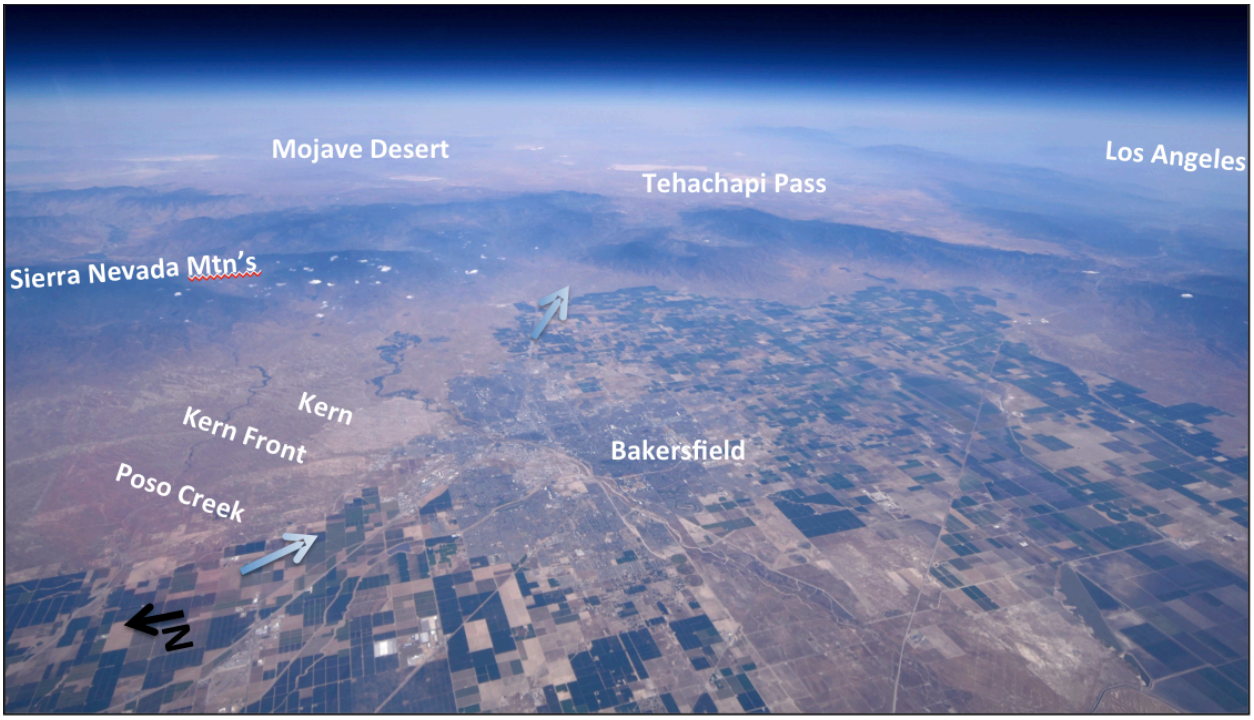


**Figure S1.** Photo of Bakersfield and the South San Joaquin Valley from the NASA (Earth Research ER-2 airplane at 20-km altitude. Blue-white arrows show approximate direction of prevailing winds, oil fields near Bakersfield labeled. Photo courtesy Stuart Broce, Pilot, NASA Armstrong Flight Research Center.

## S2. Platforms

### S2.1. Surface – AMOG Surveyor

Mobile surface *in situ* measurements using Cavity RingDown Spectroscopy (CRDS) (Pétron et al., 2012; Farrell et al., 2013) and open path spectroscopy (Sun et al., 2014) are becoming more common. Surface data were collected for the *GOSAT COMEX Experiment* by the AMOG (AutoMObile trace Gas) Surveyor (Leifer et al., 2014). AMOG Surveyor is a commuter car (Versa SP, Nissan, Japan) that is modified for mobile high-speed, high-spatial resolution observations of meteorology (winds, temperature, and pressure), gases (greenhouse and other trace), and remote sensing parameters (Fig. S2).


**Figure S2.** **(a)** AMOG Surveyor in the Transverse Coastal Range (1300 m) – San Joaquin Valley in background. **(b)** Cockpit view of gauges, security video, rear video, real-time data display. $V_A$, $V_{FB}$, $V_{RB}$, $V_I$ – voltages for alternator, front battery, rear battery, inverter. $T_I$, $T_O$, $T_{W,}$-temperatures for inverter, engine oil, and radiator water. $P_T$, $P_O$, $P_W$, $P_S$, $P_C$, $P_R$ – pressures for tires, oil, water suspension, compressor, and regulated air for chemical scrubbers. **(c)** AMOG Surveyor in Sierra Nevada Mountains, roof package labeled.

Analyzers: AMOG Surveyor draws air down two ½" PFA Teflon sample lines from 5 and 3 m above ground into a configurable range of gas analyzers by a high flow (850 lpm, 30 cfm) vacuum pump (Edwards, GVSP30). The higher sample line connects to several analyzers including a Fast-flow, enhanced performance Greenhouse Gas Analyzer (FGGA, enhanced model, Los Gatos Research an ABB Company, San Jose, CA), which uses Integrated Cavity Off-Axis Spectrometer-Cavity Enhanced Absorption Spectroscopy (ICOAS-CEAS) and measures carbon dioxide, $CO_2$, methane, $CH_4$, and water vapor, $H_2O$, at up to 10 Hz (Model 911-0010, Los Gatos Research an ABB Company, San Jose, CA). AMOG also measures carbonyl sulfide (COS) and carbon monoxide (CO) with an ICOAS-CRDS analyzer (Model 907-0028, Los Gatos Research an ABB Company, San Jose, CA). An additional sample line collects feeds an ICOAS-

CRDS that measure ammonia ($NH_3$) and hydrogen sulfide ($H_2S$). For all CEAS analyzers, dry values are used. Also, three chemiluminescence trace gas analyzers measure nitric oxide (NO) and nitrogen oxides ($NO_X$) at 0.1 Hz at 25 ppt accuracy (42TL, ThermoFischer Scientific, Waltham, MA), and ozone ($O_3$) at 0.25 Hz at 1 ppb accuracy (42C, ThermoFischer Scientific, Waltham, MA), and sulfur dioxide ($SO_2$) at 0.1 Hz at 1 ppb accuracy (450C, ThermoFischer Scientific, Waltham, MA). This accuracy is from the manufacturer and is based on 24-hour drift. Better accuracy is achieved by hourly zero gas measurements using chemically sparged air (Type CI, Cameron Great Lakes, OH), which in the laboratory improved accuracy to 50 ppt. Given that $SO_2$ and $H_2S$ atmospheric concentrations are typically less than 1 ppb in California, this was an important improvement.

The FGGA is calibrated with an air calibration standard for greenhouse gases ($CH_4$: 1.981 ppmv; $CO_2$: 404 ppmv; balance ultrapure air) and are stable to 1 ppb for CH4 over 24 hours, and 0.12 ppm for CO2 over 24 hours. Accuracy is $<$0.03%. Calibrations are performed before and after each field collect. The 49i was cross calibrated with the AJAX $O_3$ analyzer to 1 ppb, and during a repeat cross calibration several months later had maintained its calibration to between 1 and 2 ppb.

Meteorology: A sonic anemometer (VMT700, Vaisala, Finland) is mounted 1.4 m above the roof and measures two-dimensional winds. Estimated accuracy is approximately 10° and 0.3 m $s^{-1}$ for wind speeds above 1.5 m $s^{-1}$; however, accuracy improves with vehicle velocity and wind speed as vehicle flow stream line interferences are reduced. Accuracy was determined empirically by driving several kilometers back and forth on a rural road in an open area in the early morning and comparing measured winds in the two directions. Note, these accuracies are greater than the manufacturer maximum error. At lower wind speeds, accuracy appears to be closer to 0.2 m $s^{-1}$, and 15-20°; however, is extremely challenging to determine. Still, filtered nocturnal wind data generally agrees well (~10°) with expectations from topographic forcing at wind speeds of ~0.2 - 0.5 m $s^{-1}$ on large spatial scales (tens of kilometers) even at highway speed (140 km $hr^{-1}$). In general, winds are more accurate than stated if the winds are from within 30° of forward direction, as stated if they are from the side, unless strong ($>$~4 m $s^{-1}$), in which case they are equally accurate and very poor if from within ~15° of the aft direction. As a result, tail winds are not evaluated.

AMOG system improvements beyond (2014) include a high speed thermocouple (50416-T, Cooper-Atkins, CT) and a high accuracy (0.2 hPa) pressure sensor (61320V RM Young Co., MI), connected by a stainless steel line into a roof passive radiation shield (7710, Davis Instruments, CA) to reduce dynamic pressure effects. The radiation shield also includes a Type T thermocouple (Omega, CT) digitized at 0.03°C resolution (CB-7018, Measurement Computing, MA). A solar insolation sensor is digitized at 16 bit and 1 Hz (CB-7017, Measurement Computing, MA). Two (redundant) Global Navigation Satellite Systems (19X HVS, Garmin, KS) that use the GLONASS, GPS, Galileo, and QZSS satellites provide position information at 10 Hz.

Vehicle Power: To support the science package (~1.8 kW), with clean DC and AC power, AMOG has a 3.3 kW alternator (Nations Alternator, Cape Girardeau, MO), with a 2.7 kW inverter (2810M, Outback Power, Arlington, OR), and a dual voltage conversion 2.4kW uninterruptible power supply (Tripp Lite SU3000RTXL3U) backed by three, deep cycle gel batteries for a total of 250 Amp-hours (Lifeline Batteries, WI; 6FM100H, Vision, MO; PVX-1040T, Sun Xtender, CA) with active isolation (Dual Rectifier Isolator, Stolper International, Inc., San Diego, CA). The 100 A-hr batteries and inverter are mounted in the cabin floor center to improve stability. The DC system includes a 1-farad capacitor to stabilize against surges.

AMOG Surveyor weighs ~1 ton above stock, with significant safety implications, which were addressed by enhancements to handling, suspension, and braking. Specifically, front drilled and slotted ceramic brakes (F2473, Black Hart). Suspension modifications include rear airbag suspension (NV-NINV-RBK, X2 Industries, AZ), adjustable rear truck shocks (for a Ford F-150), performance coil-over front struts (TSC123, Tanabe, Japan), strut tower bar, sway bar, and ladder brace.

Data Handling and Integration: A touchscreen tablet (SpectreX360, HP) logs data asynchronously from instruments and sensors through several serial Ethernet servers (5450

NPort, Moxa, Brea, CA) and industrial switches (EDS205, Moxa, Brea, CA). Logged data are mirrored to a SSD LAN drive in AMOG. Acquisition time is identified to ~30 milliseconds from the position of the data in the serial server buffer queues.

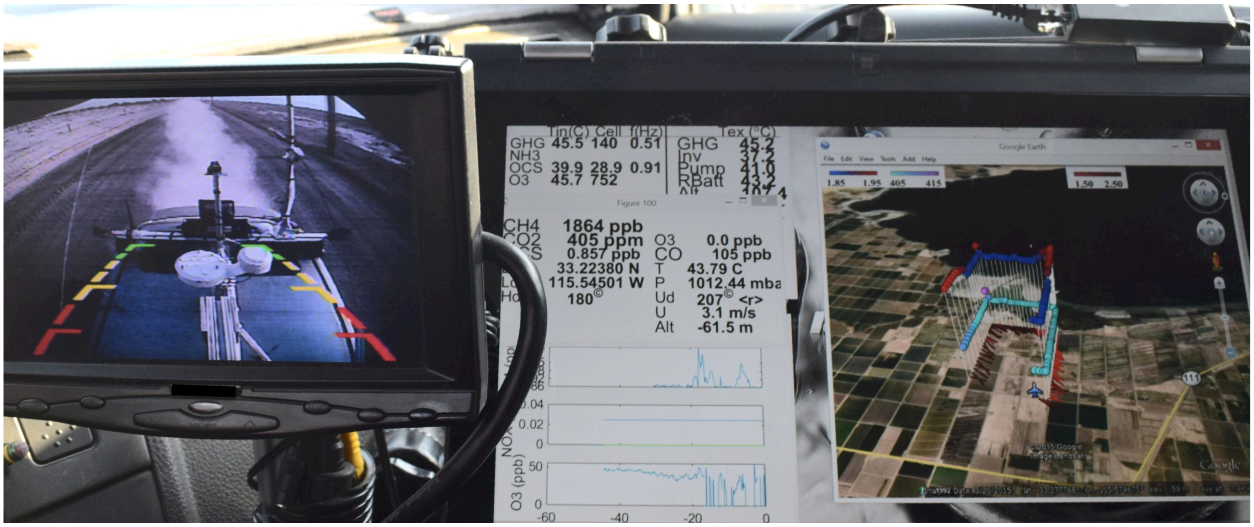


**Figure S3.** AMOG Surveyor cockpit view showing real-time display (right) and rear camera view in the Salton Sea, CA. Methane ($CH_4$) carbon dioxide ($CO_2$), and wind speed ($U$) and direction ($U_d$) are shown in the Google Earth visualization window. Rolling display (lower left) shows $CH_4$, nitrogen oxides ($NO_X$) and ozone ($O_3$). Diagnostics window (upper left) shows cell pressures and temperatures and key temperatures.

Custom software integrates the data streams and creates real time visualizations of multiple parameters in the Google Earth environment to enable adaptive surveying (Thompson et al., 2015). In adaptive surveying, the survey route is modified based on real time environmental conditions (winds, new/unexpected sources, etc.). GoogleEarth visualizations are displayed on one to several computers in AMOG Surveyor (**Fig. S3**) and remotely through cloud mirroring. Viewing algorithms automatically follow the vehicle, rotated to display wind vectors, and adjust the view altitude based on vehicle velocity. Algorithms minimize track overlap confusion through selective use of transparency. Specifically, when AMOG Surveyor returns on the same course, or loops around transparency is applied. Rolling history displays of gas concentrations are useful for identifying recently transected plumes. Other windows display AMOG Surveyor and analyzer diagnostics, and real time analyzer gas and meteorology values.

**S2.2. Airborne - AJAX**

Airborne *in situ* data were collected by AJAX (Alpha Jet Atmospheric eXperiment), operated from NASA Ames Research Center (ARC) at Moffett Field, CA. The alpha jet aircraft, which has been modified for science missions, measures carbon dioxide and methane (Picarro Inc., model G2301-m), ozone (Model 205, 2B Technologies Inc.), formaldehyde (COmpact Formaldehyde Fluorescence Experiment, COFFEE), and meteorological parameters including 3D winds by the Meteorological Measurement System (MMS), a NASA developed system (https://earthscience.arc.nasa.gov/mms), from two externally-mounted wing pods (**Fig. S4**). MMS accuracies are ±1 $m\ s^{-1}$ horizontal, 0.3 $m\ s^{-1}$ vertical. The greenhouse instrument was calibrated using whole-air (National Oceanic and Atmospheric Administration) standards before and after aircraft deployment. The ozone sensor is frequently calibrated to a NIST- traceable standard. Further details on the aircraft and instrumentation are reported by Hamill et al. (2015); Tanaka et al. (2016) and Yates et al. (2013).

**Figure S4.** AJAX photo. Courtesy Warren Gore, NASA Ames Research Center.

The Alpha Jet is owned by H211, LLC, a collaborative partner with NASA. It is a tactical strike fighter developed by Dassault-Breguet and Dornier through a German-French NATO collaboration. Dassault concurrently developed a trainer version of the Alpha Jet that is still in service with the French Air Force. Carrying a crew of two, it has a length of 12.2 m, a wingspan of 9.2 m, and a height of 4.2 m. Its empty weight is 3540 kg and a maximum takeoff weight of 8000 kg. It has a ceiling of 15,545 m, speed of 280 – 930 km $hr^{-1}$, and a range of approximately 1930 km with full fuel.

The Alpha Jet stationed at NASA Ames – Moffett Field is operated in accordance with an FAA Experimental Certificate of Airworthiness. AJAX's flight duration is 2 to 2.5 hours, permitting up to two missions per day with appropriate crew changes. Three highly experienced H211 pilots are FAA Type Certificated to fly the Alpha Jet, and science test flights began in September 2010. Following a complete avionics update and installation of the NASA-specified payload management and control system in early 2009, the Alpha Jet has proven extremely robust and reliable. Its fleet safety record as a twin-engine, all weather jet is excellent, and its modern Snecma engines produce a noise signature equivalent to current generation Stage III noise compliant turbofan aircraft.

H211 has provided significant upgrades to the aircraft to support scientific studies. Extensive wiring and cabling provisions have been installed to both wing pod locations, as well as the centerline pod, to allow for distribution of 120 and 26 volt AC and 28 volt DC to each wing pod, as well as additional 120 volt AC and 28 volt DC service to the centerline pod. Redundant heavy-duty ethernet cables have been provided from the wing pods to the centerline pod and backseat control console. An operator interface panel has been installed in the rear cockpit to allow power on/off/failure interface to each scientific instrument. Additionally, the pilot has a payload master power switch that can remove all electrical power from the NASA payloads in the event an abnormal electrical condition is encountered.

Multiple redundant Garmin G600/G530/G430/G696 systems record and display position, attitude, heading, altitude, true air speed, ground speed, true air temperature, wind speed, wind direction, and a wide variety of additional data through dual digital air data computers. This information is recorded for science use. A digital autopilot system allows highly accurate heading and track control via GPS steering, plus precise altitude control during air sampling missions. AJAX flights can also be followed in real-time using the NASA Airborne Science Mission Tool Suite.

Two wing-mounted pods have been modified by NASA-ARC to carry instrumentation, with three down-looking window ports available on each pod. Each wing pod has an approximate available volume of 0.1 cubic meter, with a maximum payload weight of 136 kg. The centerline pod has two payload areas of approximately 86.4 x 25.4 x 30.5 cm and 68.6 x 16.5 x 25.4 cm, carrying combined payloads up to 136 kg total.

**S4. Upwind Profile**

An upwind pre-survey east-west transect was conducted by AMOG from Delano (~70 m) on the floor of the San Joaquin Valley to Alta Sierra (~1750 m) on the ridge of the Greenhorne Mountains in the Sierra Nevada Mountain Range (Fig. S5). This survey passed through a range of surface topography and vegetation and canopy types. Example Google Maps "street images" show variation from flat grasslands to rolling grass covered hills, to scattered low oak trees, to at the highest altitudes, dense, tall pine forests. The road shifts from an initial gradual rise while following a primarily straight and gently curved pathway, to steeper climbs cut into steep slopes with sharp curves, and even hairpin curves.

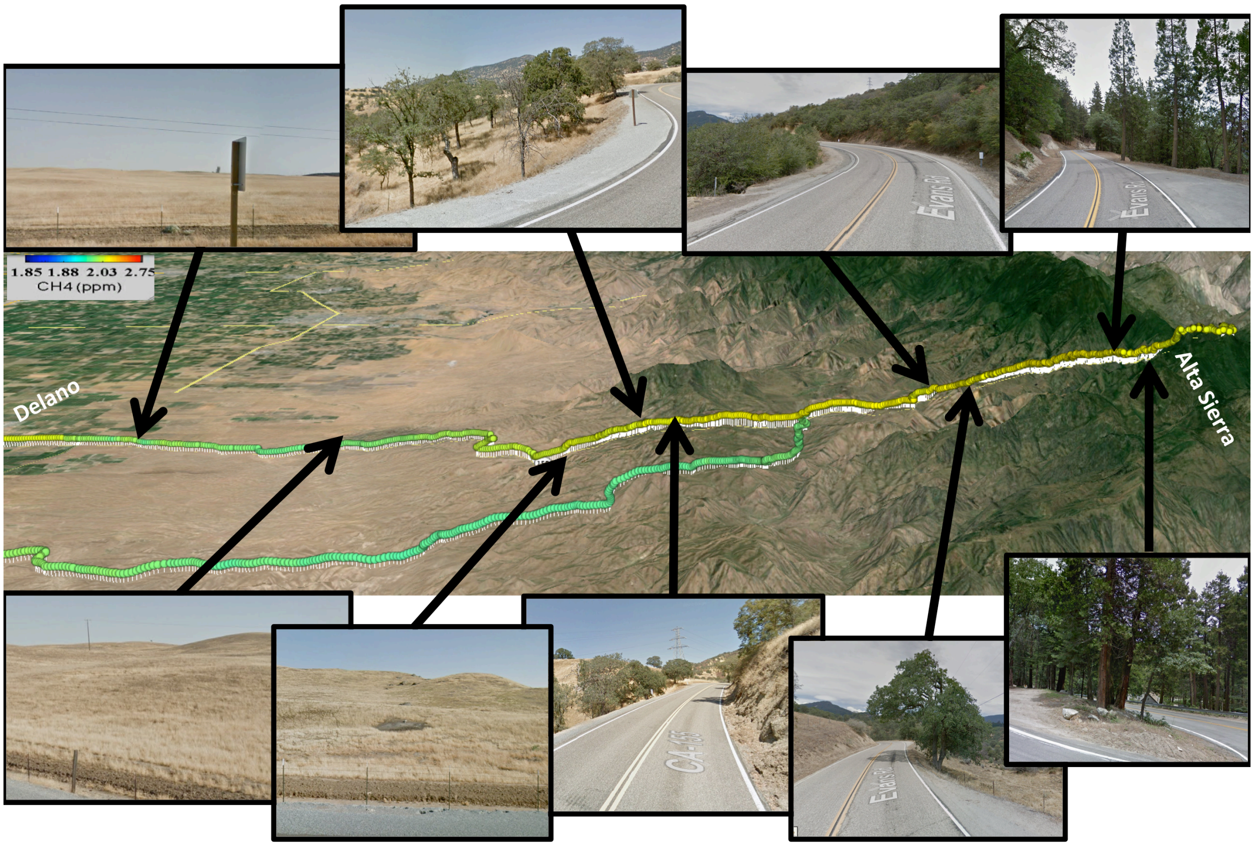


**Figure S5** – Sierra Nevada Mountain Range vertical profile, and Google maps street images showing changing terrain. Data key on figure.

## S5. Derivation of the background data curtain

The background data plane was calculated from the probability distributions on the left and on the right side of the transects at each altitude. Then, the $CH_4$ for the peak of each distribution is assigned to the left and right side of each altitude transect and linearly interpolated. Finally, the distribution is vertically interpolated to fill in the background data plane (Fig. S6).

The background data plane (Fig. S6) for transect $\gamma-\gamma'$ (Fig. 7) showed a trend of increasing $CH_4$ towards the west, rising more than ~25 ppb, at both the surface and at 480 m altitude. In contrast, background $CO_2$ across the data curtain was quite uniform.

Anomaly concentration was relative to the background concentration curtain (Fig. S6a & 6b) and was derived by estimating the background concentration at each transect altitude from fitting a

Gaussian to the background occurrence concentration distribution and using the distribution peak as the background concentration (Fig. S6c-S6f). The methodology is described in Sect. 2.4.

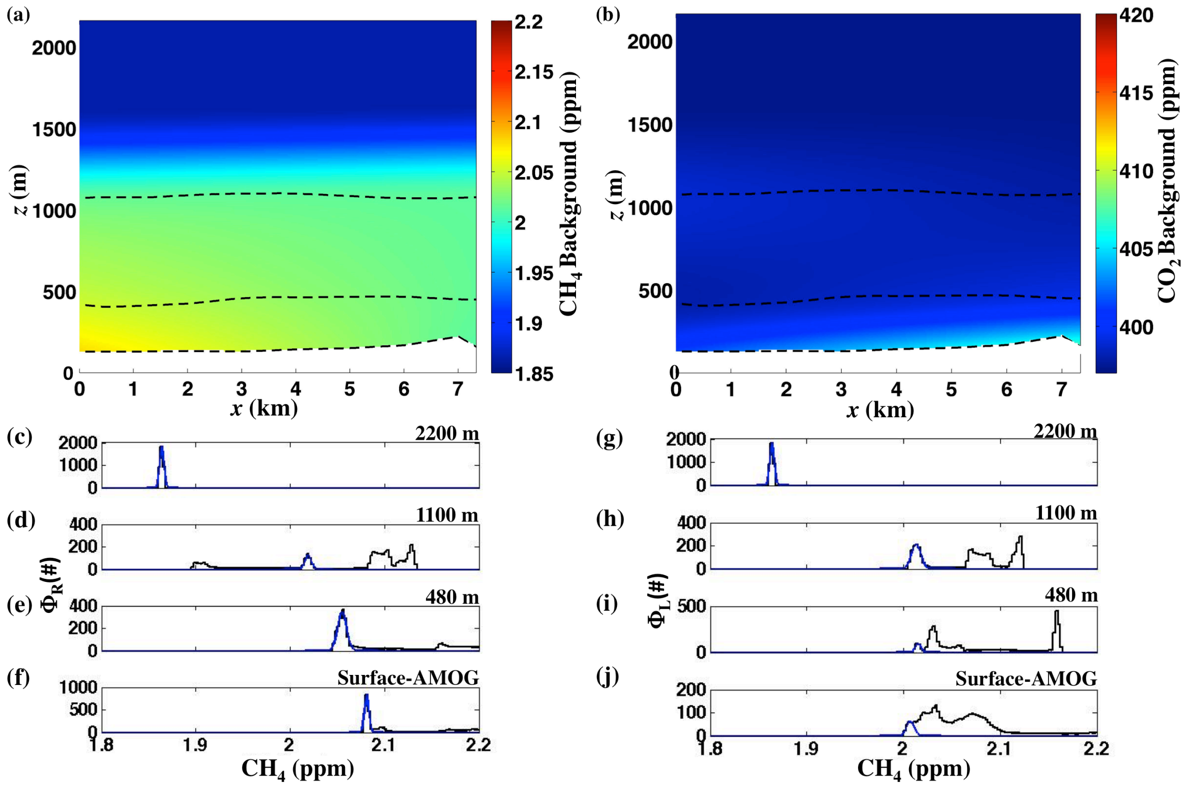


**Figure S6** – Background **(a)** methane ($CH_4$) and **(b)** carbon dioxide ($CO_2$) data curtain with respect to lateral east distance ($x$) relative to 119.0023°W, 35.3842°N for data plane γ–γ' and altitude ($z$). Dashed line shows data altitudes. **(c-f)** $CH_4$ left side probability distribution and **(g-j)** $CH_4$ right side probability distributions (Φ).

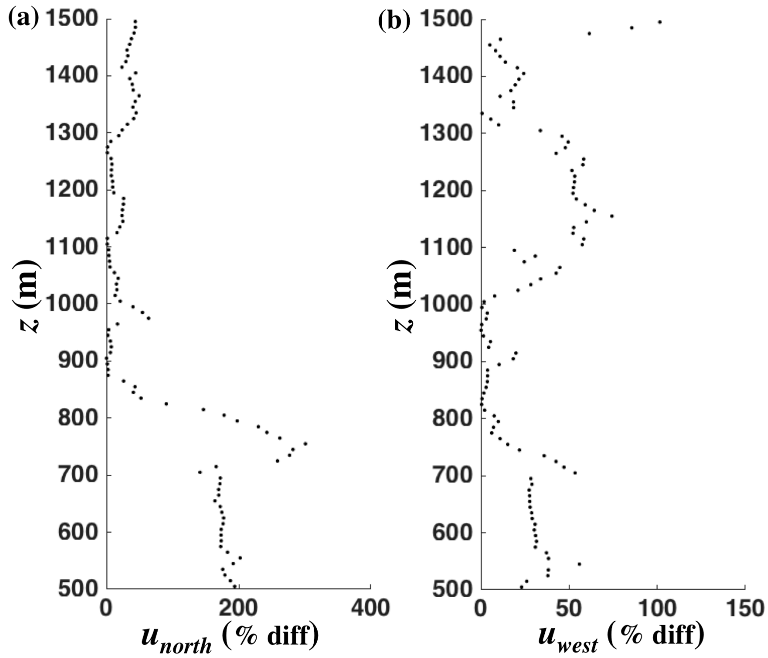


**Figure S7** – Comparison between AMOG **(a)** $u_{north}$ **(b)** and $u_{west}$.

## References

Farrell, P., Leifer, I., Culling, D., 2013. Transcontinental methane measurements: Part 1. A mobile surface platform for source investigations. Atmospheric Environment 74, 422-431, doi:10.1016/j.atmosenv.2013.02.014

Hamill, P., Iraci, L.T., Yates, E.L., Gore, W., Bui, T.P., Tanaka, T., Loewenstein, M., 2015. A new instrumented airborne platform for atmospheric research. Bulletin of the American Meteorological Society 97, doi:10.1175/BAMS-D-14-00241.1

Leifer, I., Melton, C., Manish, G., Leen, B., 2014. Mobile monitoring of methane leakage. Gases and Instrumentation July/August 2014, 20-24,

Pétron, G., Frost, G., Miller, B.R., Hirsch, A.I., Montzka, S.A., Karion, A., Trainer, M., Sweeney, C., Andrews, A.E., Miller, L., Kofler, J., Bar-Ilan, A., Dlugokencky, E.J., Patrick, L., Moore, C.T.J., Ryerson, T.B., Siso, C., Kolodzey, W., Lang, P.M., Conway, T., Novelli, P., Masarie, K., Hall, B., Guenther, D., Kitzis, D., Miller, J., Welsh, D., Wolfe, D., Neff, W., Tans, P., 2012. Hydrocarbon emissions characterization in the Colorado Front Range: A pilot study. J. Geophys. Res. 117, D04304, doi:10.1029/2011jd016360

Sun, K., Tao, L., Miller, D.J., Khan, A.M., Zondlo, M.A., 2014. On-road ammonia emissions characterized by mobile, open-path measurements. Environmental Science & Technology 48, 3943-3950, doi:10.1021/es4047704 |

Tanaka, T., Yates, E., Iraci, L.T., Johnson, M.S., Gore, W., Tadi, J.M., Loewenstein, M., Kuze, A., Frankenberg, C., Butz, A., Yoshida, Y., 2016. Two-year comparison of airborne measurements of CO<sub>2</sub> and CH<sub>4</sub> with GOSAT at Railroad Valley, Nevada. IEEE Transactions on Geoscience and Remote Sensing 54, 4367-4375, doi:10.1109/TGRS.2016.2539973

Thompson, D., Leifer, I., Bovensman, H., Eastwood, M., Fladeland, M., Frankenberg, C., Gerilowski, K., Green, R., Krautwurst, S., Krings, T., Luna, B., Thorpe, A.K., 2015. Real-time remote detection and measurement for airborne imaging spectroscopy: A case study with methane. Atmospheric Measurement Techniques 8, 1-46, doi:10.5194/amtd-8-1-2015

Yates, E.L., Iraci, L.T., Roby, M.C., Pierce, R.B., Johnson, M.S., Reddy, P.J., Tadić, J.M., Loewenstein, M., Gore, W., 2013. Airborne observations and modeling of springtime stratosphere-to-troposphere transport over California. Atmos. Chem. Phys. 13, 12481-12494, doi:10.5194/acp-13-12481-2013